

Emerging chiral optics from chiral interfaces

Xinyan Zhang^{1,2,*}, Yuhan Zhong^{1,2,*}, Tony Low^{3,†}, Hongsheng Chen^{1,2,‡}, and Xiao Lin^{1,2,§}

¹Interdisciplinary Center for Quantum Information, State Key Laboratory of Modern Optical Instrumentation, ZJU-Hangzhou Global Scientific and Technological Innovation Center, Zhejiang University, Hangzhou 310027, China

²International Joint Innovation Center; Key Lab. of Advanced Micro/Nano Electronic Devices & Smart Systems of Zhejiang, The Electromagnetics Academy at Zhejiang University, Zhejiang University, Haining 314400, China

³Department of Electrical and Computer Engineering, University of Minnesota, Minneapolis, Minnesota 55455, USA



(Received 9 December 2020; accepted 20 April 2021; published 5 May 2021)

Twisted atomic bilayers are emerging platforms for manipulating chiral light-matter interaction at the extreme nanoscale, due to their inherent magnetoelectric responses induced by the finite twist angle and quantum interlayer coupling between the atomic layers. Recent studies have reported the direct correspondence between twisted atomic bilayers and chiral metasurfaces, which features a chiral surface conductivity, in addition to the electric and magnetic surface conductivities. However, far-field chiral optics in light of these constitutive conductivities remains unexplored. Within the framework of the full Maxwell equations, we find that the chiral surface conductivity can be exploited to realize perfect polarization transformation between linearly polarized light. Remarkably, such an exotic chiral phenomenon can occur either for the reflected or transmitted light. Moreover, we reveal that all transmitted light through the judiciously designed chiral surface conductivity can always have the polarization different from the incident light, irrespective of the incident angle.

DOI: 10.1103/PhysRevB.103.195405

I. INTRODUCTION

Due to the pioneering discovery of superconducting and correlated insulating states in twisted bilayer graphene [1–5], twisted atomic bilayers have been igniting enormous research interest both in practical applications and fundamental physics [6–11], including optics with two-dimensional (2D) twistronics [12–21]. Due to the rotational misalignment and the strong quantum coupling between the neighboring atomic layers, all mirror symmetry in twisted atomic bilayers is broken, and the corresponding light-matter interaction is inherently chiral. As such, twisted atomic bilayers are emerging atomically thin platforms for chiral optics [22–28] and chiral plasmonics [29–35], which may facilitate novel on-chip applications such as the discrimination of chiral molecules with opposite handedness.

On the other hand, recent studies [34] have revealed the direct correspondence between twisted atomic bilayers and chiral metasurfaces in the framework of the full Maxwell equations. In essence, the twisted atomic bilayer is equivalent to a chiral metasurface, which simultaneously possesses the electric surface conductivity $\bar{\sigma}_e$, magnetic surface conductivity $\bar{\sigma}_m$, and chiral surface conductivity $\bar{\sigma}_\chi$. Mathematically, the electromagnetic boundary conditions for such a chiral metasurface are described by [34]

$$\hat{n} \times (\bar{E}_1 - \bar{E}_2) = -\bar{\sigma}_m(\bar{H}_1 + \bar{H}_2) + \bar{\sigma}_\chi(\bar{E}_1 + \bar{E}_2), \quad (1)$$

$$\hat{n} \times (\bar{H}_1 - \bar{H}_2) = +\bar{\sigma}_e(\bar{E}_1 + \bar{E}_2) + \bar{\sigma}_\chi(\bar{H}_1 + \bar{H}_2), \quad (2)$$

where \bar{E}_1 and \bar{E}_2 (\bar{H}_1 and \bar{H}_2) are the components of electric (magnetic) fields parallel to the boundary in the regions above the boundary (i.e., denoted as region 1) and beneath the boundary (region 2), respectively, and $\hat{n} = -\hat{z}$ is the surface normal [Fig. 1]. In principle, these surface conductivities can be arbitrary tensors, which can be constructed by stacking appropriate atomic layers (e.g., in-plane anisotropic or magnetic 2D materials) [7–9,36–39], or with regular metasurface approaches (e.g., nanopatterning) [40–44]. Recent study of chiral plasmonics as governed by Eqs. (1) and (2) [34] revealed that the chiral surface conductivity can be exploited to manifest the longitudinal spin of surface plasmons, in addition to the conventional transverse spin of surface plasmons [45–48]. Apart from this work, the field of chiral optics with the chiral surface conductivity remains relatively elusive, and exotic chiral optical phenomena remain to be discovered.

Here, we systematically investigate the far-field chiral optical phenomena with chiral interfaces due to the interplay between the chiral, electric, and magnetic surface conductivities. The general expressions for the reflection and transmission coefficients under the incidence of linearly polarized light are analytically derived. Without loss of generality and in accordance with Ref. [34], we set $\bar{\sigma}_e = [\begin{matrix} \sigma_{e,x} & 0 \\ 0 & \sigma_{e,y} \end{matrix}]$, $\bar{\sigma}_m = [\begin{matrix} \sigma_{m,x} & 0 \\ 0 & \sigma_{m,y} \end{matrix}]$ and $\bar{\sigma}_\chi = [\begin{matrix} \sigma_{\chi,x} & 0 \\ 0 & \sigma_{\chi,y} \end{matrix}]$ in this work, where each matrix element can be taken to be arbitrary values. In principle, the derivation here can be readily generalized to the cases with other forms of surface conductivities, such as those with nonzero off-diagonal terms, e.g., in systems with broken time reversal symmetry. Remarkably, we realize that all transmitted light through the ultrathin chiral interface always has the polarization different from the incident

*These authors contributed equally to this work.

†Corresponding author: tlw@umn.edu

‡Corresponding author: hansomchen@zju.edu.cn

§Corresponding author: xiaolinjz@zju.edu.cn

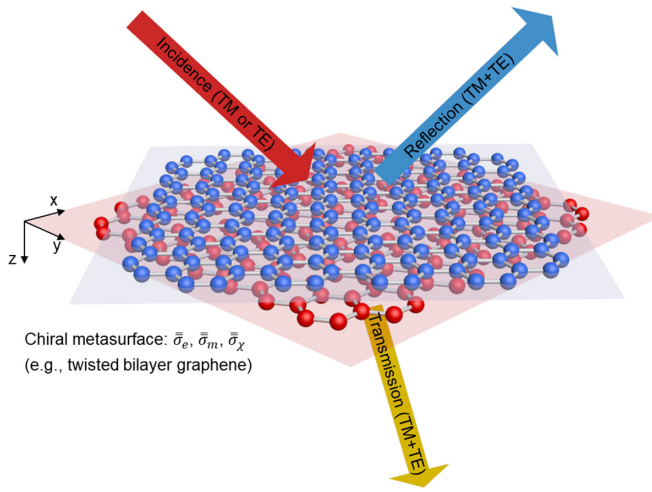


FIG. 1. Schematic of the reflection and transmission from a chiral metasurface under the incidence of linearly polarized waves. The chiral metasurface is featured with an electric surface conductivity $\bar{\sigma}_e$, a magnetic surface conductivity $\bar{\sigma}_m$, and a chiral surface conductivity $\bar{\sigma}_\chi$. The chiral metasurface is located at the boundary between region 1 ($z < 0$) and region 2 ($z > 0$). Due to the chiral response of metasurfaces, the reflected and transmitted waves generally contain both the transverse-electric (TE, or s polarized) and transverse-magnetic (TM, or p polarized) field components.

light, irrespective of the incident angle. Besides, we reveal the possibility to achieve the perfect polarization transformation between linearly polarized light in the limit when the chiral surface conductivity dominates. To be specific, this exotic chiral phenomenon can occur either in the transmission or reflection mode, if the chiral surface conductivity fulfills the condition of $\sigma_{\chi,x}\sigma_{\chi,y} = 1$ or $\sigma_{\chi,x}\sigma_{\chi,y} = -1$, respectively.

II. RESULTS AND DISCUSSION

A. Reflection and transmission from a chiral metasurface with arbitrary $\bar{\sigma}_e$, $\bar{\sigma}_m$, and $\bar{\sigma}_\chi$

We begin with the analysis of the scattering coefficients due to a chiral metasurface in the framework of the full Maxwell equations [49–52]. Due to the chiral response of chiral interfaces, the reflected and transmitted light generally has both the transverse magnetic (TM, or p polarized) and electric (TE, or s polarized) components, irrespective of the polarization of incident light; see the schematic illustration in Fig. 1. Without loss of generality, here we set the chiral metasurface to be located at the boundary (at $z = 0$) between region 1 and region 2. For region 1 (region 2), its permittivity and permeability are ϵ_1 and μ_1 (ϵ_2 and μ_2), respectively. Below we present the general solution for the reflection and transmission under the incidence of TM waves, while the corresponding solution under the incidence of TE waves is given in Appendix B.

Under the incidence of TM waves, the magnetic field of incident waves has the following form:

$$\bar{H}_i = \hat{y}e^{i\bar{k}_1\cdot\bar{r}} = \hat{y}e^{ik_x x + ik_{1z} z}, \quad (3)$$

where $\bar{k}_1 = \hat{x}k_x + \hat{z}k_{1z}$ is the wave vector of incident light in region 1. For simplicity, the incident plane is set to be parallel

to the xz plane. Since $\nabla \times \bar{H} = -i\omega\epsilon\bar{E}$ in a homogeneous isotropic media, the corresponding electric field of incident light is

$$\bar{E}_i = -\frac{k_1}{\omega\epsilon_1} \left(\hat{z}\frac{k_x}{k_1} - \hat{x}\frac{k_{1z}}{k_1} \right) e^{ik_x x + ik_{1z} z}. \quad (4)$$

The reflected and transmitted fields then take the following forms:

$$\bar{H}_r^{\text{TM}} = \hat{y}e^{ik_x x - ik_{1z} z} R_{r,\text{TM}}^{\text{i,TM}}, \quad (5)$$

$$\bar{E}_r^{\text{TM}} = -\frac{k_1}{\omega\epsilon_1} \left(\hat{z}\frac{k_x}{k_1} + \hat{x}\frac{k_{1z}}{k_1} \right) e^{ik_x x - ik_{1z} z} R_{r,\text{TM}}^{\text{i,TM}}, \quad (6)$$

$$\bar{E}_r^{\text{TE}} = \frac{k_1}{\omega\epsilon_1} \hat{y}e^{ik_x x - ik_{1z} z} R_{r,\text{TE}}^{\text{i,TM}}, \quad (7)$$

$$\bar{H}_r^{\text{TE}} = \left(\hat{z}\frac{k_x}{k_1} + \hat{x}\frac{k_{1z}}{k_1} \right) e^{ik_x x - ik_{1z} z} R_{r,\text{TE}}^{\text{i,TM}}, \quad (8)$$

$$\bar{H}_t^{\text{TM}} = \hat{y}e^{ik_x x + ik_{2z} z} T_{t,\text{TM}}^{\text{i,TM}}, \quad (9)$$

$$\bar{E}_t^{\text{TM}} = -\frac{k_2}{\omega\epsilon_2} \left(\hat{z}\frac{k_x}{k_2} - \hat{x}\frac{k_{2z}}{k_2} \right) e^{ik_x x + ik_{2z} z} T_{t,\text{TM}}^{\text{i,TM}}, \quad (10)$$

$$\bar{E}_t^{\text{TE}} = \frac{k_2}{\omega\epsilon_2} \hat{y}e^{ik_x x + ik_{2z} z} T_{t,\text{TE}}^{\text{i,TM}}, \quad (11)$$

$$\bar{H}_t^{\text{TE}} = \left(\hat{z}\frac{k_x}{k_2} - \hat{x}\frac{k_{2z}}{k_2} \right) e^{ik_x x + ik_{2z} z} T_{t,\text{TE}}^{\text{i,TM}}. \quad (12)$$

In the above equations, $\bar{k}_2 = \hat{x}k_x + \hat{z}k_{2z}$ is the wave vector of transmitted light in region 2, and we have four unknown coefficients, namely two reflection coefficients ($R_{r,\text{TM}}^{\text{i,TM}}$ and $R_{r,\text{TE}}^{\text{i,TM}}$) and two transmission coefficients ($T_{t,\text{TM}}^{\text{i,TM}}$, $T_{t,\text{TE}}^{\text{i,TM}}$). The superscript and subscript of denotes the incident polarization (i , TE or i , TM), and that of the reflected (r) and transmitted (t) light, respectively. The above scattering coefficients can be solved by enforcing the boundary conditions [53–55], i.e., by substituting Eqs. (3)–(12) into the boundary conditions governed by Eqs. (1) and (2); see details in Appendix A. Similarly, for the incidence of TE waves, the reflection coefficients ($R_{r,\text{TE}}^{\text{i,TE}}$, $R_{r,\text{TM}}^{\text{i,TE}}$) and transmission coefficients ($T_{t,\text{TE}}^{\text{i,TE}}$, $T_{t,\text{TM}}^{\text{i,TE}}$) can be obtained by following a similar procedure; see details in Appendix B.

B. Exotic polarization transformation between the incident and transmitted light for arbitrary incident angle

Although the general scattering coefficients for the far-field response of chiral metasurfaces are obtained above, these expressions are complicated and will hamper the intuitive understanding of electromagnetic phenomena. To elucidate emerging chiral phenomena, several limiting cases are considered below. First, we assume that the chiral metasurface is located in a symmetric environment (e.g., vacuum), that is, $\epsilon_1 = \epsilon_2 = \epsilon$ and $\mu_1 = \mu_2 = \mu$. Hence, we have $k_1 = k_2 = k$. Second, we let $\bar{\sigma}_e = 0$ and $\bar{\sigma}_m = 0$; see detailed discussion about the possible realization of this assumption in Appendix C. In other words, we consider the phenomenon when the chiral surface conductivity dominates over other conductivities in the problem. With these simplifications, the complexity for these reflection and transmission coefficients

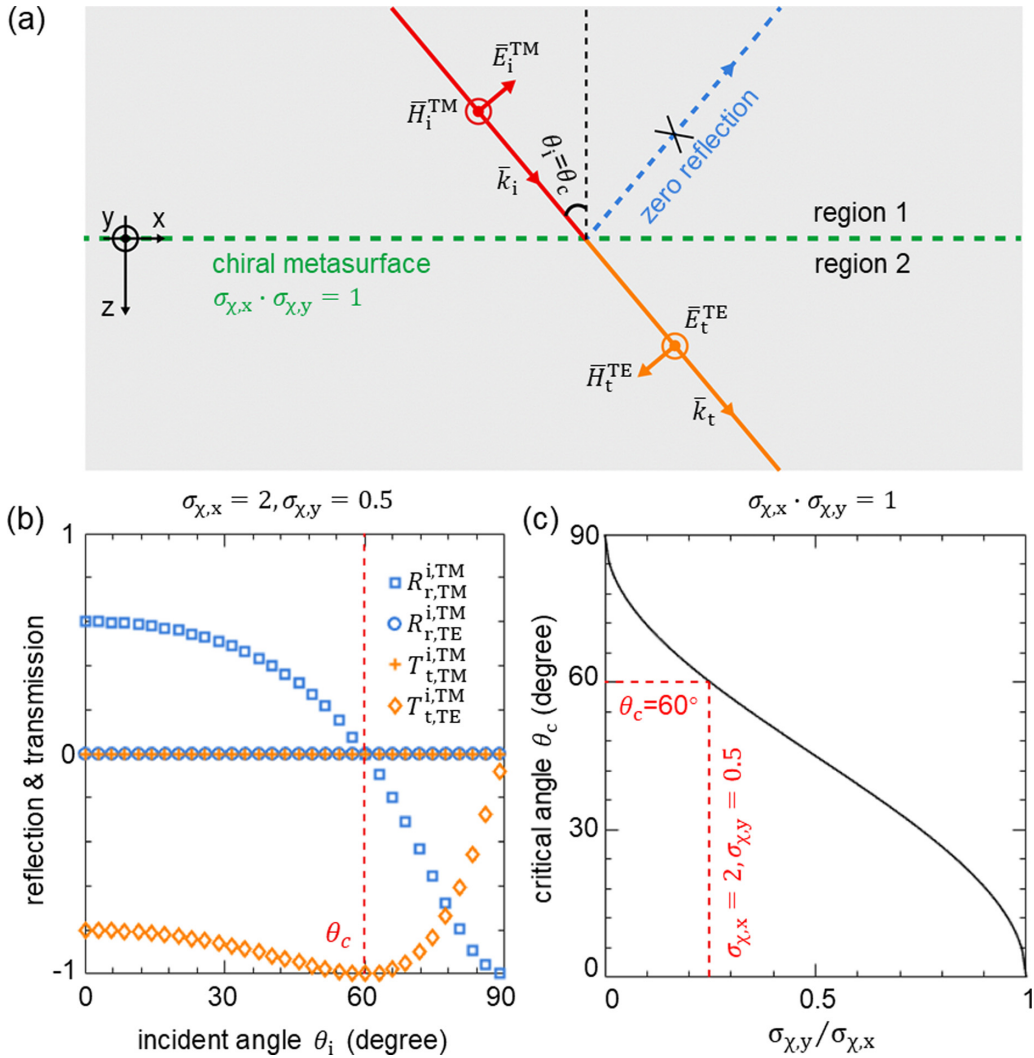


FIG. 2. Perfect polarization transformation between TM (incident) and TE (transmitted) waves. Here the chiral metasurface has $\sigma_{\chi,x}\sigma_{\chi,y} = 1$. Regions 1 and 2 are the same dielectric (e.g., vacuum used here). (a) Schematic illustration. (b) Reflection and transmission coefficients as a function of the incident angle θ_i . For conceptual demonstration, $\sigma_{\chi,x} = 2$ and $\sigma_{\chi,y} = 0.5$ are chosen. If $\sigma_{\chi,x}\sigma_{\chi,y} = 1$, $R_{r,TM}^{i,TM}$ and $T_{t,TM}^{i,TM}$ are equal to zero, irrespective of the incident angle. The critical incident angle is denoted as θ_c , at which $R_{r,TM}^{i,TM} = 0$ and $|T_{t,TM}^{i,TM}| = 1$. (c) θ_c as a function of $\sigma_{\chi,y}/\sigma_{\chi,x}$.

can be significantly reduced, as detailed in the subsequent analysis.

We consider the incidence of TM waves in Fig. 2. By applying the above simplification conditions, we readily have

$$R_{r,TM}^{i,TM} = \frac{-4\sigma_{\chi,x}\sigma_{\chi,y}(\sigma_{\chi,y} + \frac{k_z^2}{k^2}\sigma_{\chi,x})(\sigma_{\chi,y} - \frac{k_z^2}{k^2}\sigma_{\chi,x})}{(\sigma_{\chi,y} + \frac{k_z^2}{k^2}\sigma_{\chi,x})^2(1 + \sigma_{\chi,x}\sigma_{\chi,y})^2 - (\sigma_{\chi,y} - \frac{k_z^2}{k^2}\sigma_{\chi,x})^2(1 - \sigma_{\chi,x}\sigma_{\chi,y})^2}, \quad (13)$$

$$T_{t,TM}^{i,TM} = \frac{4\frac{k_z^2}{k^2}\sigma_{\chi,x}\sigma_{\chi,y}(1 + \sigma_{\chi,x}\sigma_{\chi,y})(1 - \sigma_{\chi,x}\sigma_{\chi,y})}{(\sigma_{\chi,y} + \frac{k_z^2}{k^2}\sigma_{\chi,x})^2(1 + \sigma_{\chi,x}\sigma_{\chi,y})^2 - (\sigma_{\chi,y} - \frac{k_z^2}{k^2}\sigma_{\chi,x})^2(1 - \sigma_{\chi,x}\sigma_{\chi,y})^2}, \quad (14)$$

$$R_{r,TE}^{i,TM} = \frac{-4\frac{k_z}{k}\sigma_{\chi,x}\sigma_{\chi,y}(1 - \sigma_{\chi,x}\sigma_{\chi,y})(\sigma_{\chi,y} - \frac{k_z^2}{k^2}\sigma_{\chi,x})}{(\sigma_{\chi,y} + \frac{k_z^2}{k^2}\sigma_{\chi,x})^2(1 + \sigma_{\chi,x}\sigma_{\chi,y})^2 - (\sigma_{\chi,y} - \frac{k_z^2}{k^2}\sigma_{\chi,x})^2(1 - \sigma_{\chi,x}\sigma_{\chi,y})^2}, \quad (15)$$

$$T_{t,TE}^{i,TM} = \frac{-4\frac{k_z}{k}\sigma_{\chi,x}\sigma_{\chi,y}(1 + \sigma_{\chi,x}\sigma_{\chi,y})(\sigma_{\chi,y} + \frac{k_z^2}{k^2}\sigma_{\chi,x})}{(\sigma_{\chi,y} + \frac{k_z^2}{k^2}\sigma_{\chi,x})^2(1 + \sigma_{\chi,x}\sigma_{\chi,y})^2 - (\sigma_{\chi,y} - \frac{k_z^2}{k^2}\sigma_{\chi,x})^2(1 - \sigma_{\chi,x}\sigma_{\chi,y})^2}. \quad (16)$$

Interestingly, from Eqs. (14) and (15), we always have $T_{t,TM}^{i,TM} = R_{r,TE}^{i,TM} = 0$, if

$$\sigma_{\chi,x}\sigma_{\chi,y} = 1. \quad (17)$$

Under this scenario, since $T_{t,TM}^{i,TM} = 0$ and $T_{t,TE}^{i,TM} \neq 0$, the transmitted light always has the polarization different from the incident light, indicating the occurrence of polarization transformation during the transmission process. Moreover, when Eq. (17) is satisfied, we further have $R_{r,TM}^{i,TM} = 0$ and $|R_{r,TE}^{i,TM}| = 1$ from Eqs. (13) and (16), if

$$\frac{\sigma_{\chi,y}}{\sigma_{\chi,x}} = \frac{k_z^2}{k^2}. \quad (18)$$

Remarkably, $|T_{t,TE}^{i,TM}| = 1$ indicates the occurrence of the *perfect* linear-polarization transformation between the incident and transmitted light under the incidence of TM waves; see the schematic illustration in Fig. 2(a). For clarity, the reflection and transmission coefficients are shown as a function of the incident angle θ_i in Fig. 2(b), where $\sigma_{\chi,x} = 2$ and $\sigma_{\chi,y} = 0.5$ are chosen to satisfy Eq. (17). Figure 2(b) shows that $T_{t,TM}^{i,TM} = R_{r,TE}^{i,TM} = 0$, irrespective of the incident angle. Moreover, we have $R_{r,TM}^{i,TM} = 0$ and $|T_{t,TE}^{i,TM}| = 1$ at $\theta_i = 60^\circ$ in Fig. 2(b). We denote this critical incident angle as θ_c at which the perfect polarization transformation occurs. From the geometry setup in Fig. 2(a) and Eq. (18), we have $\cos\theta_c = k_z/k = \sqrt{\frac{\sigma_{\chi,y}}{\sigma_{\chi,x}}}$. As such, the value of θ_c is simply determined by the ratio between $\sigma_{\chi,x}$ and $\sigma_{\chi,y}$, as shown in Fig. 2(c).

We highlight that previous studies about polarization transformation are focused on the perfect polarization transformation between linearly polarized light [56–58], between circularly polarized light [59–61], or between the linearly polarized and circularly polarized light [62,63], and the high-efficiency polarization transformation within a broad frequency range [64,65]. However, all these exotic phenomena of polarization transformation mainly happen at a specific incident angle or within a certain angular range of incidence [66–68], but certainly not for arbitrary incident angle. In contrast, we revealed in Fig. 2 that all transmitted light through the judiciously designed chiral interface always has the polarization different from the incident light, irrespective of the incident angle (namely the transmitted light with the polarization same as the incident light does not exist). Such an exotic phenomenon of polarization transformation for arbitrary incident angle is generally difficult to achieve by using conventional metamaterials or metasurfaces.

In addition, when $\sigma_{\chi,x}\sigma_{\chi,y} = 1$, we have $|T_{t,TE}^{i,TM}| \rightarrow 0$ and $R_{r,TM}^{i,TM} \rightarrow -1$ if $\theta_i \rightarrow 90^\circ$. This phenomenon indicates the occurrence of total reflection from chiral metasurface under the grazing incidence, which almost has no transformation of the polarization.

C. Perfect polarization transformation between the incident and reflected light

Upon close inspection of Eqs. (13)–(16), we find that the perfect polarization transformation can also happen for the reflected light under the incidence of TM waves [Fig. 3(a)], if

$$\sigma_{\chi,x}\sigma_{\chi,y} = -1, \quad (19)$$

$$\frac{\sigma_{\chi,y}}{\sigma_{\chi,x}} = -\frac{k_z^2}{k^2}. \quad (20)$$

To be specific, if $\sigma_{\chi,x}\sigma_{\chi,y} = -1$, we always have $T_{t,TM}^{i,TM} = T_{t,TE}^{i,TM} = 0$ in Eqs. (14) and (16) under the incidence of TM waves [Fig. 3(b)]. Under this scenario, the total reflection happens, irrespective of the incident angle.

Furthermore, when Eqs. (19) and (20) are simultaneously fulfilled, we further have $R_{r,TM}^{i,TM} = 0$ and $|R_{r,TE}^{i,TM}| = 1$ in Eqs. (13) and (15) at the critical incident angle $\cos\theta_c = \sqrt{-\frac{\sigma_{\chi,y}}{\sigma_{\chi,x}}}$. In other words, the perfect polarization transformation between the incident and reflected light occurs at this critical incident angle. For example, if $\sigma_{\chi,x} = 2$ and $\sigma_{\chi,y} = -0.5$, we have $|R_{r,TE}^{i,TM}| = 1$ in Fig. 3(b) at $\theta_c = 60^\circ$. In addition, a grazing angle phenomenon is also observed in Fig. 3(b), similar to that discussed for the transmission mode in Fig. 2(b).

The critical incident angle is also shown as a function of $\frac{\sigma_{\chi,y}}{\sigma_{\chi,x}}$ in Fig. 3(c). For either the reflected or transmitted light, both phenomena of the perfect polarization transformation in Figs. 2 and 3 occur at the critical angle of $\cos\theta_c = \sqrt{|\frac{\sigma_{\chi,y}}{\sigma_{\chi,x}}|}$. As such, all critical incident angles in Figs. 2(c) and 3(c) decrease from 90° to 0° when $|\frac{\sigma_{\chi,y}}{\sigma_{\chi,x}}|$ increases from 0 to 1.

Last but not least, we find that $R_{r,TE}^{i,TM} = -R_{r,TM}^{i,TE}$, $T_{t,TE}^{i,TM} = -T_{t,TM}^{i,TE}$, $R_{r,TM}^{i,TM} = +R_{r,TE}^{i,TE}$, and $T_{t,TM}^{i,TM} = +T_{t,TE}^{i,TE}$, if the above simplification conditions are adopted. Therefore, the exotic chiral phenomena in Figs. 2 and 3 can also occur under the incidence of TE waves, and the polarization of the incident light actually has no influence on the revealed phenomenon of exotic linear-polarization transformation.

III. CONCLUSION

In conclusion, we have systematically investigated the chiral optics from metasurfaces with a chiral surface conductivity under the incidence of linearly polarized light. Remarkably, we have found some emerging exotic chiral phenomena. To be specific, if $\sigma_{\chi,x}\sigma_{\chi,y} = 1$, the polarization of all transmitted light through such a chiral metasurface is distinct from that of the incident light, irrespective of the incident angle. Moreover, we can achieve the total transmittance at a critical incident angle. In contrast, if $\sigma_{\chi,x}\sigma_{\chi,y} = -1$, this type of chiral metasurfaces can be exploited to achieve total reflection instead, irrespective of the incident angle; moreover, the polarization of all reflected light can be made different from the incident light at the critical incident angle. Our work indicates the rich fundamental physics in chiral interfaces, which warrant further exploration and could find diverse chiral optical applications.

ACKNOWLEDGMENTS

The work was sponsored by the National Natural Science Foundation of China (NNSFC) under Grants No. 61625502, No. 11961141010, and No. 61975176, the Top-Notch Young Talents Program of China, the Fundamental Research Funds for the Central Universities, and Zhejiang University Global Partnership Fund. T.L. acknowledges support by the National Science Foundation, NSF/EFRI Grant No. EFRI-1741660.

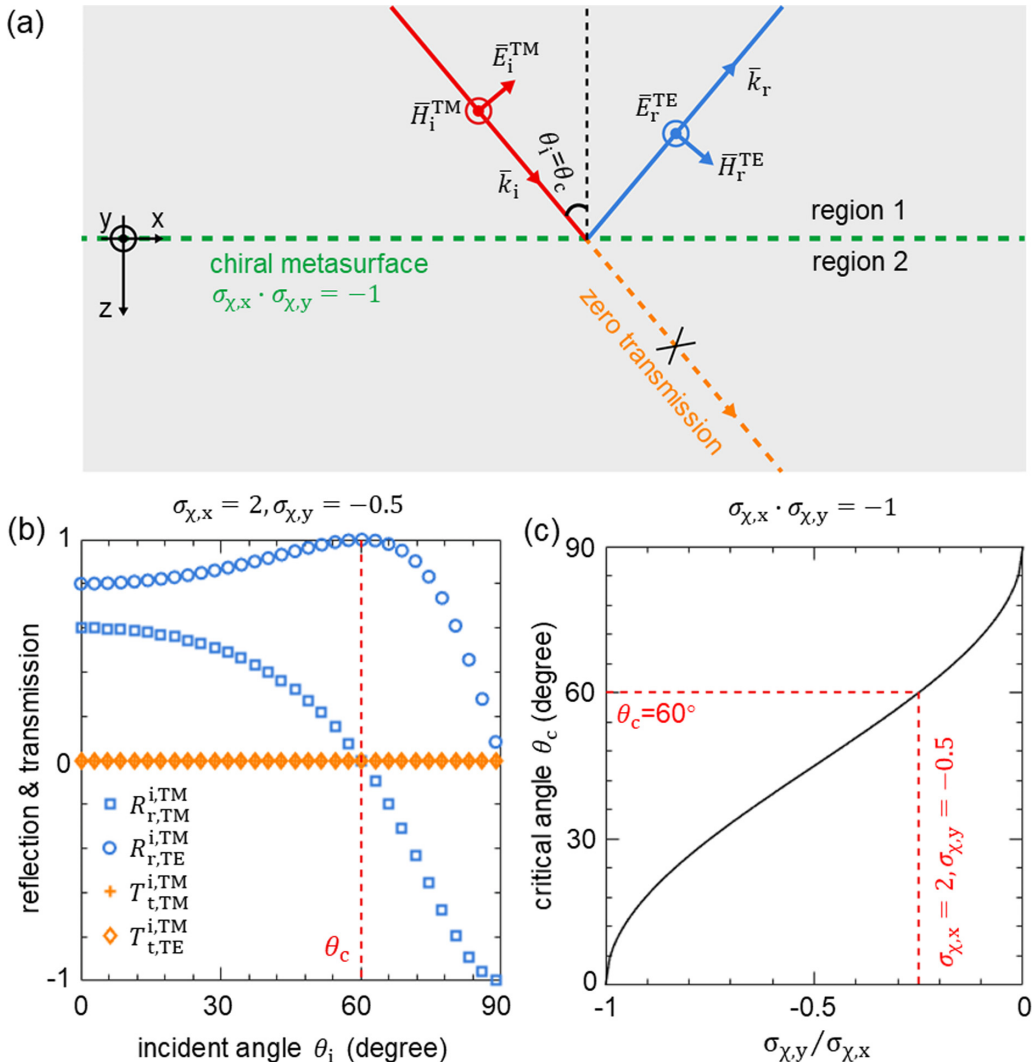


FIG. 3. Perfect polarization transformation between TM (incident) and TE (reflected) waves. The basic structural setup is the same as Fig. 2, except for that the chiral metasurface has $\sigma_{χ,x}\sigma_{χ,y} = -1$. (a) Schematic illustration. (b) Reflection and transmission coefficients as a function of θ_i . Here $\sigma_{χ,x} = 2$ and $\sigma_{χ,y} = -0.5$ are chosen for conceptual illustration. If $\sigma_{χ,x}\sigma_{χ,y} = -1$, $T_{t,\text{TE}}^{\text{i,TM}}$ and $T_{t,\text{TM}}^{\text{i,TM}}$ are equal to zero for arbitrary incident angle. The critical incident angle is denoted as θ_c , at which $R_{r,\text{TM}}^{\text{i,TM}} = 0$ and $|R_{r,\text{TE}}^{\text{i,TM}}| = 1$. (c) θ_c as a function of $\sigma_{χ,y}/\sigma_{χ,x}$.

APPENDIX A: REFLECTION AND TRANSMISSION FROM CHIRAL INTERFACES UNDER THE INCIDENCE OF TM WAVES

All reflection and transmission coefficients can be solved by enforcing the boundary conditions [53–55], i.e., by substituting Eqs. (3)–(12) into the boundary conditions governed by Eqs. (1) and (2). Then we have the relations of $R_{r,\text{TM}}^{\text{i,TM}}$, $R_{r,\text{TE}}^{\text{i,TM}}$, $T_{t,\text{TM}}^{\text{i,TM}}$, and $T_{t,\text{TE}}^{\text{i,TM}}$, as follows:

$$\begin{bmatrix} A_1^{\text{i,TM}} & B_1^{\text{i,TM}} & C_1^{\text{i,TM}} & D_1^{\text{i,TM}} \\ A_2^{\text{i,TM}} & B_2^{\text{i,TM}} & C_2^{\text{i,TM}} & D_2^{\text{i,TM}} \\ A_3^{\text{i,TM}} & B_3^{\text{i,TM}} & C_3^{\text{i,TM}} & D_3^{\text{i,TM}} \\ A_4^{\text{i,TM}} & B_4^{\text{i,TM}} & C_4^{\text{i,TM}} & D_4^{\text{i,TM}} \end{bmatrix} \begin{bmatrix} R_{r,\text{TM}}^{\text{i,TM}} \\ T_{t,\text{TM}}^{\text{i,TM}} \\ R_{r,\text{TE}}^{\text{i,TM}} \\ T_{t,\text{TE}}^{\text{i,TM}} \end{bmatrix} = \begin{bmatrix} F_1^{\text{i,TM}} \\ F_2^{\text{i,TM}} \\ F_3^{\text{i,TM}} \\ F_4^{\text{i,TM}} \end{bmatrix}, \quad (\text{A1})$$

where

$$\begin{bmatrix} A_1^{i,TM} & B_1^{i,TM} & C_1^{i,TM} & D_1^{i,TM} \\ A_2^{i,TM} & B_2^{i,TM} & C_2^{i,TM} & D_2^{i,TM} \\ A_3^{i,TM} & B_3^{i,TM} & C_3^{i,TM} & D_3^{i,TM} \\ A_4^{i,TM} & B_4^{i,TM} & C_4^{i,TM} & D_4^{i,TM} \end{bmatrix} = \begin{bmatrix} \frac{k_{1z}}{\omega\varepsilon_1} + \sigma_{m,y} & \frac{k_{2z}}{\omega\varepsilon_2} + \sigma_{m,y} & -\sigma_{\chi,y} \frac{k_1}{\omega\varepsilon_1} & -\sigma_{\chi,y} \frac{k_2}{\omega\varepsilon_2} \\ \sigma_{\chi,x} \frac{k_{1z}}{\omega\varepsilon_1} & -\sigma_{\chi,x} \frac{k_{2z}}{\omega\varepsilon_2} & \frac{k_1}{\omega\varepsilon_1} + \sigma_{m,x} \frac{k_{1z}}{k_1} & -\frac{k_2}{\omega\varepsilon_2} - \sigma_{m,x} \frac{k_{2z}}{k_2} \\ 1 + \sigma_{e,x} \frac{k_{1z}}{\omega\varepsilon_1} & -1 - \sigma_{e,x} \frac{k_{2z}}{\omega\varepsilon_2} & -\sigma_{\chi,x} \frac{k_{1z}}{k_1} & \sigma_{\chi,x} \frac{k_{2z}}{k_2} \\ \sigma_{\chi,y} & \sigma_{\chi,y} & \frac{k_{1z}}{k_1} + \sigma_{e,y} \frac{k_1}{\omega\varepsilon_1} & \frac{k_{2z}}{k_2} + \sigma_{e,y} \frac{k_2}{\omega\varepsilon_2} \end{bmatrix}, \quad (A2)$$

$$\begin{bmatrix} F_1^{i,TM} \\ F_2^{i,TM} \\ F_3^{i,TM} \\ F_4^{i,TM} \end{bmatrix} = \begin{bmatrix} \frac{k_{1z}}{\omega\varepsilon_1} - \sigma_{m,y} \\ \sigma_{\chi,x} \frac{k_{1z}}{\omega\varepsilon_1} \\ -1 + \sigma_{e,x} \frac{k_{1z}}{\omega\varepsilon_1} \\ -\sigma_{\chi,x} \end{bmatrix}. \quad (A3)$$

Then, the analytical expressions for $R_{r,TM}^{i,TM}$, $R_{r,TE}^{i,TM}$, $T_{t,TM}^{i,TM}$, and $T_{t,TE}^{i,TM}$ are obtained by solving Eq. (A1):

$$R_{r,TM}^{i,TM} = \frac{(\alpha_1^{i,TM} Q_1^{i,TM} - \beta_1^{i,TM} N_1^{i,TM}) / G^{i,TM}}{S^{i,TM}}, \quad (A4)$$

$$T_{t,TM}^{i,TM} = \frac{(\beta_1^{i,TM} M_1^{i,TM} - \alpha_1^{i,TM} P_1^{i,TM}) / G^{i,TM}}{S^{i,TM}}, \quad (A5)$$

$$R_{r,TE}^{i,TM} = \frac{(\alpha_2^{i,TM} Q_2^{i,TM} - \beta_2^{i,TM} N_2^{i,TM}) / K^{i,TM}}{S^{i,TM}}, \quad (A6)$$

$$T_{t,TE}^{i,TM} = \frac{(\beta_2^{i,TM} M_2^{i,TM} - \alpha_2^{i,TM} P_2^{i,TM}) / K^{i,TM}}{S^{i,TM}}, \quad (A7)$$

where

$$\alpha_1^{i,TM} = (F_1^{i,TM} C_2^{i,TM} - F_2^{i,TM} C_1^{i,TM})(D_3^{i,TM} C_4^{i,TM} - D_4^{i,TM} C_3^{i,TM}) - (F_3^{i,TM} C_4^{i,TM} - F_4^{i,TM} C_3^{i,TM})(D_1^{i,TM} C_2^{i,TM} - D_2^{i,TM} C_1^{i,TM}), \quad (A8)$$

$$\beta_1^{i,TM} = (F_1^{i,TM} D_2^{i,TM} - F_2^{i,TM} D_1^{i,TM})(C_3^{i,TM} D_4^{i,TM} - C_4^{i,TM} D_3^{i,TM}) - (F_3^{i,TM} D_4^{i,TM} - F_4^{i,TM} D_3^{i,TM})(C_1^{i,TM} D_2^{i,TM} - C_2^{i,TM} D_1^{i,TM}), \quad (A9)$$

$$M_1^{i,TM} = (A_1^{i,TM} C_2^{i,TM} - A_2^{i,TM} C_1^{i,TM})(D_3^{i,TM} C_4^{i,TM} - D_4^{i,TM} C_3^{i,TM}) - (A_3^{i,TM} C_4^{i,TM} - A_4^{i,TM} C_3^{i,TM})(D_1^{i,TM} C_2^{i,TM} - D_2^{i,TM} C_1^{i,TM}), \quad (A10)$$

$$N_1^{i,TM} = (B_1^{i,TM} C_2^{i,TM} - B_2^{i,TM} C_1^{i,TM})(D_3^{i,TM} C_4^{i,TM} - D_4^{i,TM} C_3^{i,TM}) - (B_3^{i,TM} C_4^{i,TM} - B_4^{i,TM} C_3^{i,TM})(D_1^{i,TM} C_2^{i,TM} - D_2^{i,TM} C_1^{i,TM}), \quad (A11)$$

$$P_1^{i,TM} = (A_1^{i,TM} D_2^{i,TM} - A_2^{i,TM} D_1^{i,TM})(C_3^{i,TM} D_4^{i,TM} - C_4^{i,TM} D_3^{i,TM}) - (A_3^{i,TM} D_4^{i,TM} - A_4^{i,TM} D_3^{i,TM})(C_1^{i,TM} D_2^{i,TM} - C_2^{i,TM} D_1^{i,TM}), \quad (A12)$$

$$Q_1^{i,TM} = (B_1^{i,TM} D_2^{i,TM} - B_2^{i,TM} D_1^{i,TM})(C_3^{i,TM} D_4^{i,TM} - C_4^{i,TM} D_3^{i,TM}) - (B_3^{i,TM} D_4^{i,TM} - B_4^{i,TM} D_3^{i,TM})(C_1^{i,TM} D_2^{i,TM} - C_2^{i,TM} D_1^{i,TM}), \quad (A13)$$

$$\alpha_2^{i,TM} = (F_1^{i,TM} A_2^{i,TM} - F_2^{i,TM} A_1^{i,TM})(B_3^{i,TM} A_4^{i,TM} - B_4^{i,TM} A_3^{i,TM}) - (F_3^{i,TM} A_4^{i,TM} - F_4^{i,TM} A_3^{i,TM})(B_1^{i,TM} A_2^{i,TM} - B_2^{i,TM} A_1^{i,TM}), \quad (A14)$$

$$\beta_2^{i,TM} = (F_1^{i,TM} B_2^{i,TM} - F_2^{i,TM} B_1^{i,TM})(A_3^{i,TM} B_4^{i,TM} - A_4^{i,TM} B_3^{i,TM}) - (F_3^{i,TM} B_4^{i,TM} - F_4^{i,TM} B_3^{i,TM})(A_1^{i,TM} B_2^{i,TM} - A_2^{i,TM} B_1^{i,TM}), \quad (A15)$$

$$M_2^{i,TM} = (C_1^{i,TM} A_2^{i,TM} - C_2^{i,TM} A_1^{i,TM})(B_3^{i,TM} A_4^{i,TM} - B_4^{i,TM} A_3^{i,TM}) - (C_3^{i,TM} A_4^{i,TM} - C_4^{i,TM} A_3^{i,TM})(B_1^{i,TM} A_2^{i,TM} - B_2^{i,TM} A_1^{i,TM}), \quad (A16)$$

$$N_2^{i,TM} = (D_1^{i,TM} A_2^{i,TM} - D_2^{i,TM} A_1^{i,TM})(B_3^{i,TM} A_4^{i,TM} - B_4^{i,TM} A_3^{i,TM}) - (D_3^{i,TM} A_4^{i,TM} - D_4^{i,TM} A_3^{i,TM})(B_1^{i,TM} A_2^{i,TM} - B_2^{i,TM} A_1^{i,TM}), \quad (A17)$$

$$P_2^{i,TM} = (C_1^{i,TM} B_2^{i,TM} - C_2^{i,TM} B_1^{i,TM})(A_3^{i,TM} B_4^{i,TM} - A_4^{i,TM} B_3^{i,TM}) - (C_3^{i,TM} B_4^{i,TM} - C_4^{i,TM} B_3^{i,TM})(A_1^{i,TM} B_2^{i,TM} - A_2^{i,TM} B_1^{i,TM}), \quad (A18)$$

$$Q_2^{i,TM} = (D_1^{i,TM}B_2^{i,TM} - D_2^{i,TM}B_1^{i,TM})(A_3^{i,TM}B_4^{i,TM} - A_4^{i,TM}B_3^{i,TM}) - (D_3^{i,TM}B_4^{i,TM} - D_4^{i,TM}B_3^{i,TM})(A_1^{i,TM}B_2^{i,TM} - A_2^{i,TM}B_1^{i,TM}), \quad (A19)$$

$$G^{i,TM} = (C_1^{i,TM}D_2^{i,TM} - C_2^{i,TM}D_1^{i,TM})(C_3^{i,TM}D_4^{i,TM} - C_4^{i,TM}D_3^{i,TM}), \quad (A20)$$

$$K^{i,TM} = (B_1^{i,TM}A_2^{i,TM} - B_2^{i,TM}A_1^{i,TM})(A_3^{i,TM}B_4^{i,TM} - A_4^{i,TM}B_3^{i,TM}), \quad (A21)$$

$$S^{i,TM} = \frac{M_1^{i,TM}Q_1^{i,TM} - P_1^{i,TM}N_1^{i,TM}}{G^{i,TM}} = \frac{M_2^{i,TM}Q_2^{i,TM} - P_2^{i,TM}N_2^{i,TM}}{K^{i,TM}}. \quad (A22)$$

APPENDIX B: REFLECTION AND TRANSMISSION FROM CHIRAL INTERFACES UNDER THE INCIDENCE OF TE WAVES

By following a similar procedure in Eqs. (3)–(12), we can calculate the reflection and transmission of light from a chiral metasurface under the incidence of TE waves. To be specific, the electric field of incident TE waves has

$$\bar{E}_i = \hat{y}e^{i\bar{k}_1 \cdot \bar{r}} = \hat{y}e^{ik_x x + ik_{1z} z}, \quad (B1)$$

where the wave vector of incident light is $\bar{k}_1 = \hat{x}k_x + \hat{z}k_{1z}$. Correspondingly, the magnetic field of incident light has

$$\bar{H}_i = \frac{k_1}{\omega\mu_1} \left(\hat{z}\frac{k_x}{k_1} - \hat{x}\frac{k_{1z}}{k_1} \right) e^{ik_x x + ik_{1z} z}. \quad (B2)$$

The reflected and transmitted fields then take the following forms:

$$\bar{E}_r^{TE} = \hat{y}e^{ik_x x - ik_{1z} z} R_{r,TE}^{i,TE}, \quad (B3)$$

$$\bar{H}_r^{TE} = \frac{k_1}{\omega\mu_1} \left(\hat{z}\frac{k_x}{k_1} + \hat{x}\frac{k_{1z}}{k_1} \right) e^{ik_x x - ik_{1z} z} R_{r,TE}^{i,TE}, \quad (B4)$$

$$\bar{H}_r^{TM} = \frac{k_1}{\omega\mu_1} \hat{y}e^{ik_x x - ik_{1z} z} R_{r,TM}^{i,TE}, \quad (B5)$$

$$\bar{E}_r^{TM} = - \left(\hat{z}\frac{k_x}{k_1} + \hat{x}\frac{k_{1z}}{k_1} \right) e^{ik_x x - ik_{1z} z} R_{r,TM}^{i,TE}, \quad (B6)$$

$$\bar{E}_t^{TE} = \hat{y}e^{ik_x x + ik_{2z} z} T_{t,TE}^{i,TE}, \quad (B7)$$

$$\bar{H}_t^{TE} = \frac{k_2}{\omega\mu_2} \left(\hat{z}\frac{k_x}{k_2} - \hat{x}\frac{k_{2z}}{k_2} \right) e^{ik_x x + ik_{2z} z} T_{t,TE}^{i,TE}, \quad (B8)$$

$$\bar{H}_t^{TM} = \frac{k_2}{\omega\mu_2} \hat{y}e^{ik_x x + ik_{2z} z} T_{t,TM}^{i,TE}, \quad (B9)$$

$$\bar{E}_t^{TM} = - \left(\hat{z}\frac{k_x}{k_2} - \hat{x}\frac{k_{2z}}{k_2} \right) e^{ik_x x + ik_{2z} z} T_{t,TM}^{i,TE}, \quad (B10)$$

where the wave vector of transmitted light is $\bar{k}_2 = \hat{x}k_x + \hat{z}k_{2z}$. The four coefficients, namely $R_{r,TE}^{i,TE}$ and $R_{r,TM}^{i,TE}$ (reflection coefficients) and $T_{t,TE}^{i,TE}$ and $T_{t,TM}^{i,TE}$ (transmission coefficients), can be solved by enforcing the boundary conditions of Eqs. (1) and (2) in the main text. By substituting Eqs. (B1)–(B10) into Eqs. (1) and (2), we obtain the relation of these coefficients as follows:

$$\begin{bmatrix} A_1^{i,TM} & B_1^{i,TM} & C_1^{i,TM} & D_1^{i,TM} \\ A_2^{i,TM} & B_2^{i,TM} & C_2^{i,TM} & D_2^{i,TM} \\ A_3^{i,TM} & B_3^{i,TM} & C_3^{i,TM} & D_3^{i,TM} \\ A_4^{i,TM} & B_4^{i,TM} & C_4^{i,TM} & D_4^{i,TM} \end{bmatrix} \begin{bmatrix} R_{r,TM}^{i,TE} \\ T_{t,TM}^{i,TE} \\ R_{r,TE}^{i,TE} \\ T_{t,TE}^{i,TE} \end{bmatrix} = \begin{bmatrix} F_1^{i,TE} \\ F_2^{i,TE} \\ F_3^{i,TE} \\ F_4^{i,TE} \end{bmatrix}, \quad (B11)$$

where

$$\begin{bmatrix} A_1^{i,TE} & B_1^{i,TE} & C_1^{i,TE} & D_1^{i,TE} \\ A_2^{i,TE} & B_2^{i,TE} & C_2^{i,TE} & D_2^{i,TE} \\ A_3^{i,TE} & B_3^{i,TE} & C_3^{i,TE} & D_3^{i,TE} \\ A_4^{i,TE} & B_4^{i,TE} & C_4^{i,TE} & D_4^{i,TE} \end{bmatrix} = \begin{bmatrix} 1 + \sigma_{m,x} \frac{k_{1z}}{\omega\mu_1} & -1 - \sigma_{m,x} \frac{k_{2z}}{\omega\mu_2} & \sigma_{\chi,x} \frac{k_{1z}}{k_1} & -\sigma_{\chi,x} \frac{k_{2z}}{k_2} \\ \sigma_{\chi,y} & \sigma_{\chi,x} & -\sigma_{m,y} \frac{k_1}{\omega\mu_1} - \frac{k_{1z}}{k_1} & -\sigma_{m,y} \frac{k_2}{\omega\mu_2} - \frac{k_{2z}}{k_2} \\ \sigma_{e,y} + \frac{k_{1z}}{\omega\mu_1} & \sigma_{e,y} + \frac{k_{2z}}{\omega\mu_2} & \sigma_{\chi,y} \frac{k_1}{\omega\mu_1} & \sigma_{\chi,y} \frac{k_2}{\omega\mu_2} \\ \sigma_{\chi,x} \frac{k_{1z}}{\omega\mu_1} & -\sigma_{\chi,x} \frac{k_{2z}}{\omega\mu_2} & -\frac{k_1}{\omega\mu_1} - \sigma_{e,x} \frac{k_{1z}}{k_1} & \frac{k_2}{\omega\mu_2} + \sigma_{e,x} \frac{k_{2z}}{k_2} \end{bmatrix}, \quad (B12)$$

$$\begin{bmatrix} F_1^{i,TE} \\ F_2^{i,TE} \\ F_3^{i,TE} \\ F_4^{i,TE} \end{bmatrix} = \begin{bmatrix} -1 + \sigma_{m,x} \frac{k_{1z}}{\omega\mu_1} \\ -\sigma_{\chi,x} \\ \frac{k_{1z}}{\omega\mu_1} - \sigma_{e,y} \\ \sigma_{\chi,x} \frac{k_{1z}}{\omega\mu_1} \end{bmatrix}. \quad (B13)$$

$R_{r,TE}^{i,TE}$, $R_{r,TM}^{i,TE}$, $T_{t,TE}^{i,TE}$, and $T_{t,TM}^{i,TE}$ then can be solved from Eq. (A12). They are expressed as follows:

$$R_{r,TE}^{i,TE} = \frac{(\alpha_1^{i,TE} Q_1^{i,TE} - \beta_1^{i,TE} N_1^{i,TE}) / G^{i,TE}}{S^{i,TE}}, \quad (B14)$$

$$T_{t,TE}^{i,TE} = \frac{(\beta_1^{i,TE} M_1^{i,TE} - \alpha_1^{i,TE} P_1^{i,TE}) / G^{i,TE}}{S^{i,TE}}, \quad (B15)$$

$$R_{r,TM}^{i,TE} = \frac{(\alpha_2^{i,TE} Q_2^{i,TE} - \beta_2^{i,TE} N_2^{i,TE}) / K^{i,TE}}{S^{i,TE}}, \quad (B16)$$

$$T_{t,TM}^{i,TE} = \frac{(\beta_2^{i,TE} M_2^{i,TE} - \alpha_2^{i,TE} P_2^{i,TE}) / K^{i,TE}}{S^{i,TE}}, \quad (B17)$$

where

$$\alpha_1^{i,TE} = (F_1^{i,TE} C_2^{i,TE} - F_2^{i,TE} C_1^{i,TE})(D_3^{i,TE} C_4^{i,TE} - D_4^{i,TE} C_3^{i,TE}) - (F_3^{i,TE} C_4^{i,TE} - F_4^{i,TE} C_3^{i,TE})(D_1^{i,TE} C_2^{i,TE} - D_2^{i,TE} C_1^{i,TE}), \quad (B18)$$

$$\beta_1^{i,TE} = (F_1^{i,TE} D_2^{i,TE} - F_2^{i,TE} D_1^{i,TE})(C_3^{i,TE} D_4^{i,TE} - C_4^{i,TE} D_3^{i,TE}) - (F_3^{i,TE} D_4^{i,TE} - F_4^{i,TE} D_3^{i,TE})(C_1^{i,TE} D_2^{i,TE} - C_2^{i,TE} D_1^{i,TE}), \quad (B19)$$

$$M_1^{i,TE} = (A_1^{i,TE} C_2^{i,TE} - A_2^{i,TE} C_1^{i,TE})(D_3^{i,TE} C_4^{i,TE} - D_4^{i,TE} C_3^{i,TE}) - (A_3^{i,TE} C_4^{i,TE} - A_4^{i,TE} C_3^{i,TE})(D_1^{i,TE} C_2^{i,TE} - D_2^{i,TE} C_1^{i,TE}), \quad (B20)$$

$$N_1^{i,TE} = (B_1^{i,TE} C_2^{i,TE} - B_2^{i,TE} C_1^{i,TE})(D_3^{i,TE} C_4^{i,TE} - D_4^{i,TE} C_3^{i,TE}) - (B_3^{i,TE} C_4^{i,TE} - B_4^{i,TE} C_3^{i,TE})(D_1^{i,TE} C_2^{i,TE} - D_2^{i,TE} C_1^{i,TE}), \quad (B21)$$

$$P_1^{i,TE} = (A_1^{i,TE} D_2^{i,TE} - A_2^{i,TE} D_1^{i,TE})(C_3^{i,TE} D_4^{i,TE} - C_4^{i,TE} D_3^{i,TE}) - (A_3^{i,TE} D_4^{i,TE} - A_4^{i,TE} D_3^{i,TE})(C_1^{i,TE} D_2^{i,TE} - C_2^{i,TE} D_1^{i,TE}), \quad (B22)$$

$$Q_1^{i,TE} = (B_1^{i,TE} D_2^{i,TE} - B_2^{i,TE} D_1^{i,TE})(C_3^{i,TE} D_4^{i,TE} - C_4^{i,TE} D_3^{i,TE}) - (B_3^{i,TE} D_4^{i,TE} - B_4^{i,TE} D_3^{i,TE})(C_1^{i,TE} D_2^{i,TE} - C_2^{i,TE} D_1^{i,TE}), \quad (B23)$$

$$\alpha_2^{i,TE} = (F_1^{i,TE} A_2^{i,TE} - F_2^{i,TE} A_1^{i,TE})(B_3^{i,TE} A_4^{i,TE} - B_4^{i,TE} A_3^{i,TE}) - (F_3^{i,TE} A_4^{i,TE} - F_4^{i,TE} A_3^{i,TE})(B_1^{i,TE} A_2^{i,TE} - B_2^{i,TE} A_1^{i,TE}), \quad (B24)$$

$$\beta_2^{i,TE} = (F_1^{i,TE} B_2^{i,TE} - F_2^{i,TE} B_1^{i,TE})(A_3^{i,TE} B_4^{i,TE} - A_4^{i,TE} B_3^{i,TE}) - (F_3^{i,TE} B_4^{i,TE} - F_4^{i,TE} B_3^{i,TE})(A_1^{i,TE} B_2^{i,TE} - A_2^{i,TE} B_1^{i,TE}), \quad (B25)$$

$$M_2^{i,TE} = (C_1^{i,TE} A_2^{i,TE} - C_2^{i,TE} A_1^{i,TE})(B_3^{i,TE} A_4^{i,TE} - B_4^{i,TE} A_3^{i,TE}) - (C_3^{i,TE} A_4^{i,TE} - C_4^{i,TE} A_3^{i,TE})(B_1^{i,TE} A_2^{i,TE} - B_2^{i,TE} A_1^{i,TE}), \quad (B26)$$

$$N_2^{i,TE} = (D_1^{i,TE} A_2^{i,TE} - D_2^{i,TE} A_1^{i,TE})(B_3^{i,TE} A_4^{i,TE} - B_4^{i,TE} A_3^{i,TE}) - (D_3^{i,TE} A_4^{i,TE} - D_4^{i,TE} A_3^{i,TE})(B_1^{i,TE} A_2^{i,TE} - B_2^{i,TE} A_1^{i,TE}), \quad (B27)$$

$$P_2^{i,TE} = (C_1^{i,TE} B_2^{i,TE} - C_2^{i,TE} B_1^{i,TE})(A_3^{i,TE} B_4^{i,TE} - A_4^{i,TE} B_3^{i,TE}) - (C_3^{i,TE} B_4^{i,TE} - C_4^{i,TE} B_3^{i,TE})(A_1^{i,TE} B_2^{i,TE} - A_2^{i,TE} B_1^{i,TE}), \quad (B28)$$

$$Q_2^{i,TE} = (D_1^{i,TE} B_2^{i,TE} - D_2^{i,TE} B_1^{i,TE})(A_3^{i,TE} B_4^{i,TE} - A_4^{i,TE} B_3^{i,TE}) - (D_3^{i,TE} B_4^{i,TE} - D_4^{i,TE} B_3^{i,TE})(A_1^{i,TE} B_2^{i,TE} - A_2^{i,TE} B_1^{i,TE}), \quad (B29)$$

$$G^{i,TE} = (C_1^{i,TE} D_2^{i,TE} - C_2^{i,TE} D_1^{i,TE})(C_3^{i,TE} D_4^{i,TE} - C_4^{i,TE} D_3^{i,TE}), \quad (B30)$$

$$K^{i,TE} = (B_1^{i,TE} A_2^{i,TE} - B_2^{i,TE} A_1^{i,TE})(A_3^{i,TE} B_4^{i,TE} - A_4^{i,TE} B_3^{i,TE}), \quad (B31)$$

$$S^{i,TE} = \frac{M_1^{i,TE} Q_1^{i,TE} - P_1^{i,TE} N_1^{i,TE}}{G^{i,TE}} = \frac{M_2^{i,TE} Q_2^{i,TE} - P_2^{i,TE} N_2^{i,TE}}{K^{i,TE}}. \quad (B32)$$

If the simplification conditions (i.e. $\varepsilon_1 = \varepsilon_2 = \varepsilon$, $\mu_1 = \mu_2 = \mu$, $\bar{\sigma}_e = 0$, and $\bar{\sigma}_m = 0$) are adopted in the calculation, the expression for the scattering coefficients in Eqs. (B15)–(B18) can be significantly simplified. Under these simplification conditions, we have

$$R_{r,TE}^{i,TE} = \frac{-4\sigma_{\chi,x}\sigma_{\chi,y}(\sigma_{\chi,y} + \frac{k^2}{k^2}\sigma_{\chi,x})(\sigma_{\chi,y} - \frac{k^2}{k^2}\sigma_{\chi,x})}{(\sigma_{\chi,y} + \frac{k^2}{k^2}\sigma_{\chi,x})^2(1 + \sigma_{\chi,x}\sigma_{\chi,y})^2 - (\sigma_{\chi,y} - \frac{k^2}{k^2}\sigma_{\chi,x})^2(1 - \sigma_{\chi,x}\sigma_{\chi,y})^2}, \quad (B33)$$

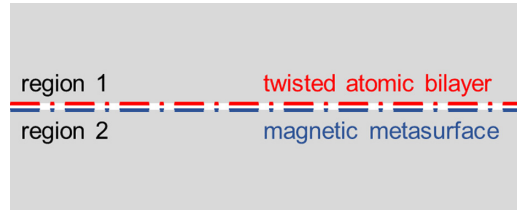


FIG. 4. Schematic illustration of the hybrid chiral structure constructed by the twisted atomic bilayer and the uniaxial magnetic metasurface.

$$T_{t,TE}^{i,TE} = \frac{4\sigma_{\chi,x}\sigma_{\chi,y}\frac{k_z^2}{k^2}(1 + \sigma_{\chi,x}\sigma_{\chi,y})(1 - \sigma_{\chi,x}\sigma_{\chi,y})}{(\sigma_{\chi,y} + \frac{k_z^2}{k^2}\sigma_{\chi,x})^2(1 + \sigma_{\chi,x}\sigma_{\chi,y})^2 - (\sigma_{\chi,y} - \frac{k_z^2}{k^2}\sigma_{\chi,x})^2(1 - \sigma_{\chi,x}\sigma_{\chi,y})^2}, \quad (B34)$$

$$R_{r,TM}^{i,TE} = \frac{4\frac{k_z}{k}\sigma_{\chi,x}\sigma_{\chi,y}(\sigma_{\chi,y} - \frac{k_z^2}{k^2}\sigma_{\chi,x})(1 - \sigma_{\chi,x}\sigma_{\chi,y})}{(\sigma_{\chi,y} + \frac{k_z^2}{k^2}\sigma_{\chi,x})^2(1 + \sigma_{\chi,x}\sigma_{\chi,y})^2 - (\sigma_{\chi,y} - \frac{k_z^2}{k^2}\sigma_{\chi,x})^2(1 - \sigma_{\chi,x}\sigma_{\chi,y})^2}, \quad (B35)$$

$$T_{t,TM}^{i,TE} = \frac{4\frac{k_z}{k}\sigma_{\chi,x}\sigma_{\chi,y}(\sigma_{\chi,y} + \frac{k_z^2}{k^2}\sigma_{\chi,x})(1 + \sigma_{\chi,x}\sigma_{\chi,y})}{(\sigma_{\chi,y} + \frac{k_z^2}{k^2}\sigma_{\chi,x})^2(1 + \sigma_{\chi,x}\sigma_{\chi,y})^2 - (\sigma_{\chi,y} - \frac{k_z^2}{k^2}\sigma_{\chi,x})^2(1 - \sigma_{\chi,x}\sigma_{\chi,y})^2}. \quad (B36)$$

APPENDIX C: A FEASIBLE WAY TO ACHIEVE THE CONDITION OF $\bar{\bar{\sigma}}_e = 0$, $\bar{\bar{\sigma}}_m = 0$, and $\bar{\bar{\sigma}}_\chi \neq 0$

As schematically shown in Fig. 4, the hybrid structure constructed by the twisted atomic bilayer and a uniaxial magnetic metasurface can in principle help to achieve the above condition. To be specific, according to our previous work [34], the twisted atomic bilayer (TAB) is equivalent to a chiral metasurface, which simultaneously has the electric ($\bar{\bar{\sigma}}_{e,TAB}$), magnetic ($\bar{\bar{\sigma}}_{m,TAB}$), and chiral ($\bar{\bar{\sigma}}_{\chi,TAB}$) surface conductivities. These effective surface conductivities are all 2×2 diagonal matrices, and particularly, we have $\bar{\bar{\sigma}}_\chi = -\sigma_{xy}\bar{\bar{\sigma}}_m$ [34]. On the other hand, for the uniaxial magnetic metasurface, it can be readily modeled by the electric ($\bar{\bar{\sigma}}_{e,META}$) and magnetic ($\bar{\bar{\sigma}}_{m,META}$) surface conductivities, which are also both 2×2 diagonal matrices. Then if we deposit this uniaxial magnetic metasurface very close to the twisted atomic bilayer, the effective total surface conductivities for this hybrid structure can be approximately characterized by $\bar{\bar{\sigma}}_{e,\text{total}} = \bar{\bar{\sigma}}_{e,META} + \bar{\bar{\sigma}}_{e,TAB}$, $\bar{\bar{\sigma}}_{m,\text{total}} = \bar{\bar{\sigma}}_{m,META} + \bar{\bar{\sigma}}_{m,TAB}$, and $\bar{\bar{\sigma}}_{\chi,\text{total}} = \bar{\bar{\sigma}}_{\chi,TAB}$. As such, through judiciously designing $\bar{\bar{\sigma}}_{e,META}$ and $\bar{\bar{\sigma}}_{m,META}$, we can obtain $\bar{\bar{\sigma}}_{e,\text{total}} = 0$ and $\bar{\bar{\sigma}}_{m,\text{total}} = 0$, while keeping $\bar{\bar{\sigma}}_{\chi,\text{total}} \neq 0$.

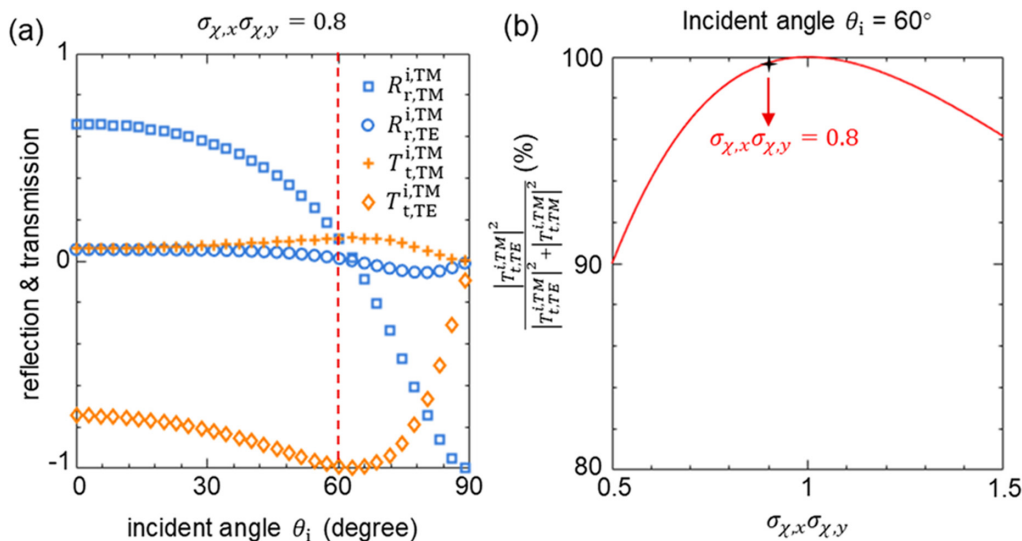


FIG. 5. Influence of imperfections on the polarization transformation between the incident and transmitted light. All basic setup here are the same as Fig. 2, except for the value of $\sigma_{\chi,x}\sigma_{\chi,y}$. As a typical example of imperfection, here we set $\sigma_{\chi,x}\sigma_{\chi,y} \neq 1$. (a) Reflection and transmission coefficients as a function of the incident angle under the scenario of $\sigma_{\chi,x}\sigma_{\chi,y} = 0.8$. (b) Proportion of TE waves among all transmitted waves as a function of $\sigma_{\chi,x}\sigma_{\chi,y}$. Here the incident light is TM polarized (same as Fig. 2), and we set the incident angle to be 60° , namely the critical incident angle at which the perfection polarization transformation happens in Fig. 2.

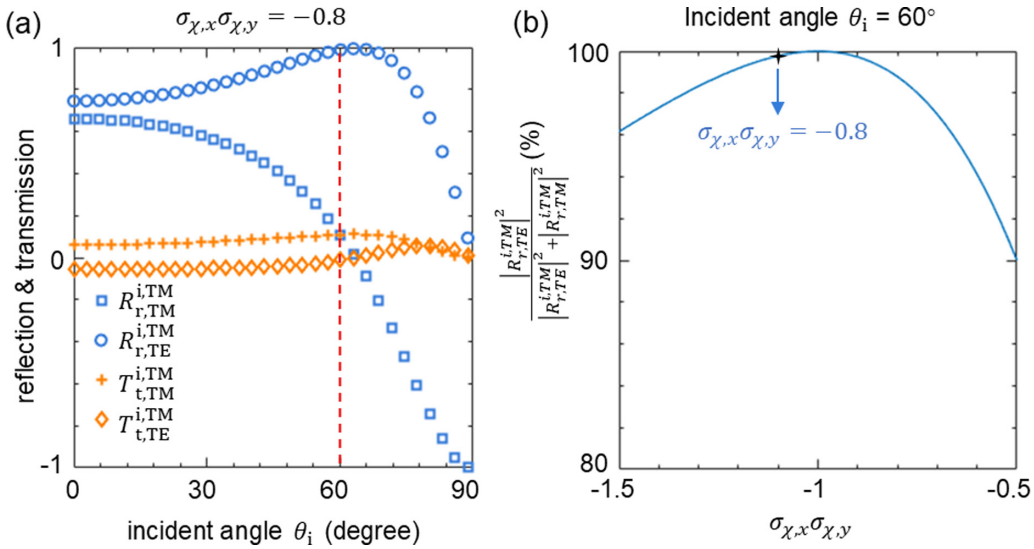


FIG. 6. Influence of imperfections on the polarization transformation between the incident and reflected light. The basic setup here is the same as Fig. 3, except for the value of $\sigma_{χ,x}\sigma_{χ,y}$. As a typical example of imperfection, here we set $\sigma_{χ,x}\sigma_{χ,y} \neq -1$. (a) Reflection and transmission coefficients as a function of the incident angle under the scenario of $\sigma_{χ,x}\sigma_{χ,y} = -0.8$. (b) Proportion of TE waves among all reflected waves as a function of $\sigma_{χ,x}\sigma_{χ,y}$. Here the incident light is TM polarized (same as Fig. 3), and we set the incident angle to be 60° , namely the critical incident angle at which the perfect polarization transformation happens in Fig. 3.

APPENDIX D: INFLUENCE OF IMPERFECTION ON THE POLARIZATION TRANSFORMATION

As a typical example of imperfection, below we set $|\sigma_{χ,x}\sigma_{χ,y}| \neq 1$ and discuss its influence on the polarization transformation. For the exotic polarization transformation between the incident (TE) and transmitted (TM) waves revealed in Fig. 2, Fig. 5(a) shows that if $|\sigma_{χ,x}\sigma_{χ,y}| \neq 1$ (e.g., $\sigma_{χ,x}\sigma_{χ,y} = 0.8$), we can still have that most of the transmitted light has the polarization different from the incident light, irrespective of the incident angle. As a further quantitative study, we show in Fig. 5(b) that at the critical incident angle (at which the perfect polarization transformation happens in Fig. 2), the proportion of TM waves among all transmitted light is always above 90%, when $\sigma_{χ,x}\sigma_{χ,y}$ varies from 0.5 to 1.5. Similarly, for the perfect polarization transformation between the incident (TM) and reflected (TE) light revealed in Fig. 3, Fig. 6 shows that at the critical incident angle, the proportion of TM waves among all reflected light is also always above 90%, when $\sigma_{χ,x}\sigma_{χ,y}$ varies from 0.5 to 1.5.

-
- [1] Y. Cao, V. Fatemi, A. Demir, S. Fang, S. L. Tomarken, J. Y. Luo, J. D. Sanchez-Yamagishi, K. Watanabe, T. Taniguchi, E. Kaxiras, R. C. Ashoori, and P. Jarillo-Herrero, Correlated insulator behaviour at half-filling in magic-angle graphene superlattices, *Nature (London)* **556**, 80 (2018).
 - [2] Y. Cao, V. Fatemi, S. Fang, K. Watanabe, T. Taniguchi, E. Kaxiras, and P. Jarillo-Herrero, Unconventional superconductivity in magic-angle graphene superlattices, *Nature (London)* **556**, 43 (2018).
 - [3] Y. Choi, J. Kemmer, Y. Peng, A. Thomson, H. Arora, R. Polski, Y. Zhang, H. Ren, J. Alicea, G. Refael, F. von Oppen, K. Watanabe, T. Taniguchi, and S. Nadj-Perge, Electronic correlations in twisted bilayer graphene near the magic angle, *Nat. Phys.* **15**, 1174 (2019).
 - [4] Y. Jiang, X. Lai, K. Watanabe, T. Taniguchi, K. Haule, J. Mao, and E. Y. Andrei, Charge order and broken rotational symmetry in magic-angle twisted bilayer graphene, *Nature (London)* **573**, 91 (2019).
 - [5] A. Kerelsky, L. J. McGillly, D. M. Kennes, L. Xian, M. Yankowitz, S. Chen, T. Taniguchi, K. Watanabe, J. Hone, C. Dean, A. Rubio, and A. N. Pasupathy, Maximized electron interactions at the magic angle in twisted bilayer graphene, *Nature (London)* **572**, 95 (2019).
 - [6] R. Bistritzer and A. H. MacDonald, Moiré bands in twisted double-layer graphene, *Proc. Natl. Acad. Sci. USA* **108**, 12233 (2011).
 - [7] C. R. Dean, L. Wang, P. Maher, C. Forsythe, F. Ghahari, Y. Gao, J. Katoch, M. Ishigami, P. Moon, M. Koshino, T. Taniguchi, K. L. Shepard, K. Watanabe, J. Hone, and P. Kim, Hofstadter's butterfly and the fractal quantum Hall effect in moiré superlattices, *Nature (London)* **497**, 598 (2013).
 - [8] J. Kunstmann, F. Mooshamer, P. Nagler, A. Chaves, F. Stein, N. Paradiso, G. Plechinger, C. Strunk, C. Schüller, G. Seifert, D. R. Reichman, and T. Korn, Momentum-space indirect interlayer excitons in transition-metal dichalcogenide van der Waals heterostructures, *Nat. Phys.* **14**, 801 (2018).
 - [9] K. Tran, G. Moody, F. Wu, X. Lu, J. Choi, K. Kim, A. Rai, D. A. Sanchez, J. Quan, A. Singh, J. Embley, A. Zepeda, M. Campbell, T. Autry, T. Taniguchi, K. Watanabe, N. Lu, S. K. Banerjee, K. L. Silverman, S. Kim, E. Tutuc, L. Yang, A. H.

- Macdonald, and X. Li, Evidence for moiré excitons in van der Waals heterostructures, *Nature (London)* **567**, 71 (2019).
- [10] A. L. Sharpe, E. J. Fox, A. W. Barnard, J. Finney, K. Watanabe, T. Taniguchi, M. A. Kastner, and D. Goldhaber-Gordon, Emergent ferromagnetism near three-quarters filling in twisted bilayer graphene, *Science* **365**, 605 (2019).
- [11] J. Mao, S. P. Milovanović, M. Andelković, X. Lai, Y. Cao, K. Watanabe, T. Taniguchi, L. Covaci, F. M. Peeters, A. K. Geim, Y. Jiang, and E. Y. Andrei, Evidence of flat bands and correlated states in buckled graphene superlattices, *Nature (London)* **584**, 215 (2020).
- [12] T. N. Ikeda, High-order nonlinear optical response of a twisted bilayer graphene, *Phys. Rev. Res.* **2**, 032015(R) (2020).
- [13] B. Deng, C. Ma, Q. Wang, S. Yuan, K. Watanabe, T. Taniguchi, F. Zhang, and F. Xia, Strong mid-infrared photoresponse in small-twist-angle bilayer graphene, *Nat. Photonics* **14**, 549 (2020).
- [14] M. Renuka, X. Lin, Z. Wang, L. Shen, B. Zheng, H. Wang, and H. Chen, Dispersion engineering of hyperbolic plasmons in bilayer 2D materials, *Opt. Lett.* **43**, 5737 (2018).
- [15] G. Hu, A. Krasnok, Y. Mazor, C.-W. Qiu, and A. Alù, Moiré hyperbolic metasurfaces, *Nano Lett.* **20**, 3217 (2020).
- [16] G. Hu, Q. Ou, G. Si, Y. Wu, J. Wu, Z. Dai, A. Krasnok, Y. Mazor, Q. Zhang, Q. Bao, C. Qiu, and A. Alù, Topological polaritons and photonic magic angles in twisted α -MoO₃ bilayers, *Nature (London)* **582**, 209 (2020).
- [17] M. Chen, X. Lin, T. H. Dinh, Z. Zheng, J. Shen, Q. Ma, H. Chen, P. Jarillo-Herrero, and S. Dai, Configurable Phonon polaritons in α -MoO₃ bilayers, *Nat. Mater.* **19**, 1307 (2020).
- [18] J. Duan, N. Capote-Robayna, J. Taboada-Gutiérrez, G. Álvarez-Pérez, I. Prieto, J. Martín-Sánchez, A. Y. Nikitin, and P. Alonso-González, Twisted nano-optics: Manipulating light at the nanoscale with twisted phonon polaritonic slabs, *Nano Lett.* **20**, 5323 (2020).
- [19] Z. Zheng, F. Sun, W. Huang, J. Jiang, R. Zhan, Y. Ke, H. Chen, and S. Deng, Phonon polaritons in twisted double-layers of hyperbolic van der Waals crystals, *Nano Lett.* **20**, 5301 (2020).
- [20] Q. Fu, P. Wang, C. Huang, Y. V. Kartashov, L. Torner, V. V. Konotop, and F. Ye, Optical soliton formation controlled by angle twisting in photonic moiré lattices, *Nat. Photonics* **14**, 663 (2020).
- [21] W. J. M. Kort-Kamp, F. J. Culchac, R. B. Capaz, and F. A. Pinheiro, Photonic spin Hall effect in bilayer graphene moiré superlattices, *Phys. Rev. B* **98**, 195431 (2018).
- [22] C. J. Tabert and E. J. Nicol, Optical conductivity of twisted bilayer graphene, *Phys. Rev. B* **87**, 121402(R) (2013).
- [23] C. Kim, A. Sánchez-Castillo, Z. Ziegler, Y. Ogawa, C. Noguez, and J. Park, Chiral atomically thin films, *Nat. Nanotechnol.* **11**, 520 (2016).
- [24] T. Cao, Z. Li, D. Y. Qiu, and S. G. Louie, Gate switchable transport and optical anisotropy in 90° twisted bilayer black phosphorus, *Nano Lett.* **16**, 5542 (2016).
- [25] T. Stauber, T. Low, and G. Gómez-Santos, Chiral Response of Twisted Bilayer Graphene, *Phys. Rev. Lett.* **120**, 046801 (2018).
- [26] T. Stauber, T. Low, and G. Gómez-Santos, Linear response of twisted bilayer graphene: Continuum versus tight-binding models, *Phys. Rev. B* **98**, 195414 (2018).
- [27] Z. Addison, J. Park, and E. J. Mele, Twist, slip, and circular dichroism in bilayer graphene, *Phys. Rev. B* **100**, 125418 (2019).
- [28] H. Ochoa and A. Asenjo-Garcia, Flat Bands and Chiral Optical Response of Moiré Insulators, *Phys. Rev. Lett.* **125**, 037402 (2020).
- [29] G. X. Ni, H. Wang, J. S. Wu, Z. Fei, M. D. Goldflam, F. Keilmann, B. Özyilmaz, A. H. Castro Neto, X. M. Xie, M. M. Fogler, and D. N. Basov, Plasmons in graphene moiré superlattices, *Nat. Mater.* **14**, 1217 (2015).
- [30] F. Hu, S. R. Das, Y. Luan, T.-F. Chung, Y. P. Chen, and Z. Fei, Real-Space Imaging of the Tailored Plasmons in Twisted Bilayer Graphene, *Phys. Rev. Lett.* **119**, 247402 (2017).
- [31] S. S. Sunku, G. X. Ni, B. Y. Jiang, H. Yoo, A. Sternbach, A. S. McLeod, T. Stauber, L. Xiong, T. Taniguchi, K. Watanabe, P. Kim, M. M. Fogler, and D. N. Basov, Photonic crystals for nano-light in moiré graphene superlattices, *Science* **362**, 1153 (2018).
- [32] T. Stauber and H. Kohler, Quasi-flat plasmonic bands in twisted bilayer graphene, *Nano Lett.* **16**, 6844 (2016).
- [33] C. Lewandowski and L. Levitov, Intrinsically undamped plasmon modes in narrow electron bands, *Proc. Natl. Acad. Sci.* **116**, 20869 (2019).
- [34] X. Lin, Z. Liu, T. Stauber, G. Gómez-Santos, F. Gao, and H. Chen, Chiral Plasmons with Twisted Atomic Bilayers, *Phys. Rev. Lett.* **125**, 077401 (2020).
- [35] P. Novelli, I. Torre, F. H. L. Koppens, F. Taddei, and M. Polini, Optical and plasmonic properties of twisted bilayer graphene: Impact of interlayer tunneling asymmetry and ground-state charge inhomogeneity, *Phys. Rev. B* **102**, 125403 (2020).
- [36] T. Low, A. Chaves, J. D. Caldwell, A. Kumar, N. X. Fang, P. Avouris, T. F. Heinz, F. Guinea, L. Martin-Moreno, and F. Koppens, Polaritons in layered two-dimensional materials, *Nat. Mater.* **16**, 182 (2017).
- [37] T. Low, R. Roldán, H. Wang, F. Xia, P. Avouris, L. M. Moreno, and F. Guinea, Plasmons and Screening in Monolayer and Multilayer Black Phosphorus, *Phys. Rev. Lett.* **113**, 106802 (2014).
- [38] A. Chaves, J. G. Azadani, H. Alsalman, D. R. da Costa, R. Frisenda, A. J. Chaves, S. H. Song, Y. D. Kim, D. He, J. Zhou, A. Castellanos-Gómez, F. M. Peeters, Z. Liu, C. L. Hinkle, S.-H. Oh, P. D. Ye, S. J. Koester, Y. H. Lee, P. Avouris, X. Wang, and T. Low, Bandgap engineering of two-dimensional semiconductor materials, *npj 2D Mater. Appl.* **4**, 29 (2020).
- [39] J. B. Harley, M. U. Saleh, S. Kingston, M. A. Scarpulla, and C. M. Furse, Fast transient simulations for multi-segment transmission lines with a graphical model, *Progress in Electromagnetics Research* **165**, 67 (2019).
- [40] Y. Fan, N. Shen, F. Zhang, Q. Zhao, Z. Wei, P. Zhang, J. Dong, Q. Fu, H. Li, and C. M. Soukoulis, Photoexcited graphene metasurfaces: Significantly enhanced and tunable magnetic resonances, *ACS Photonics* **5**, 1612 (2018).
- [41] M. Li, L. Jing, X. Lin, S. Xu, L. Shen, B. Zheng, Z. Wang, and H. Chen, Angular-adaptive spin-locked retroreflector based on reconfigurable magnetic metagrating, *Adv. Opt. Mater.* **7**, 1900151 (2019).
- [42] Y. Li, Y. Xu, M. Jiang, B. Li, T. Han, C. Chi, F. Lin, B. Shen, X. Zhu, L. Lai, and Z. Fang, Self-Learning Perfect Optical Chirality Via a Deep Neural Network, *Phys. Rev. Lett.* **123**, 213902 (2019).

- [43] W. Ma, Z. Liu, Z. A. Kudyshev, A. Boltasseva, W. Cai, and Y. Liu, Deep learning for the design of photonic structures, *Nat. Photonics* **15**, 77 (2021).
- [44] J. Zhang, X. Hu, H. Chen, and F. Gao, Designer surface plasmons enable Terahertz Cherenkov radiation, *Progress in Electromagnetics Research* **169**, 25 (2020).
- [45] X. Shi, X. Lin, I. Kaminer, F. Gao, Z. Yang, J. D. Joannopoulos, M. Soljačić, and B. Zhang, Superlight inverse Doppler effect, *Nat. Phys.* **14**, 1001 (2018).
- [46] X. Lin and B. Zhang, Normal Doppler frequency shift in negative refractive-index systems, *Laser Photonics Rev.* **13**, 1900081 (2019).
- [47] K. Y. Bliokh and F. Nori, Transverse spin of a surface polariton, *Phys. Rev. A* **85**, 061801(R) (2012).
- [48] K. Y. Bliokh, F. J. Rodríguez-Fortuño, F. Nori, and A. V. Zayats, Spin-orbit interactions of light, *Nat. Photonics* **9**, 796 (2015).
- [49] X. Zhang, H. Hu, X. Lin, L. Shen, B. Zhang, and H. Chen, Confined transverse-electric graphene plasmons in negative refractive-index systems, *npj 2D Mater. Appl.* **4**, 25 (2020).
- [50] C. Wang, C. Qian, H. Hu, L. Shen, Z. Wang, H. Wang, Z. Xu, B. Zhang, H. Chen, and X. Lin, Superscattering of light in refractive-index near-zero environments, *Progress in Electromagnetics Research* **168**, 15 (2020).
- [51] L. Shen, X. Lin, M. Y. Shalaginov, T. Low, X. Zhang, B. Zhang, and H. Chen, Broadband enhancement of on-chip single-photon extraction via tilted hyperbolic metamaterials, *Appl. Phys. Rev.* **7**, 021403 (2020).
- [52] C. Valagiannopoulos, Designing nanoinclusions for quantum sensing based on electromagnetic scattering formalism, *Progress in Electromagnetics Research* **170**, 1 (2021).
- [53] X. Lin, I. Kaminer, X. Shi, F. Gao, Z. Yang, Z. Gao, H. Buljan, J. D. Joannopoulos, M. Soljačić, H. Chen, and B. Zhang, Splashing transients of 2D plasmons launched by swift electrons, *Sci. Adv.* **3**, e1601192 (2017).
- [54] X. Lin, S. Easo, Y. Shen, H. Chen, B. Zhang, J. D. Joannopoulos, M. Soljačić, and I. Kaminer, Controlling Cherenkov angles with resonance transition radiation, *Nat. Phys.* **14**, 816 (2018).
- [55] H. Hu, X. Lin, J. Zhang, D. Liu, P. Genevet, B. Zhang, and Y. Luo, Nonlocality induced Cherenkov threshold, *Laser Photonics Rev.* **14**, 2000149 (2020).
- [56] Y. Cheng, W. Li, and X. Mao, Triple-band polarization angle independent 90° polarization rotator based on Fermat's spiral structure planar chiral metamaterial, *Progress in Electromagnetics Research* **165**, 35 (2019).
- [57] N. K. Grady, J. E. Heyes, D. R. Chowdhury, Y. Zeng, M. T. Reiten, A. K. Azad, A. J. Taylor, D. A. R. Dalvit, and H.-T. Chen, Terahertz metamaterials for linear polarization conversion and anomalous refraction, *Science* **340**, 1304 (2013).
- [58] J. Hao, Y. Yuan, L. Ran, T. Jiang, J. A. Kong, C. T. Chan, and L. Zhou, Manipulating Electromagnetic Wave Polarizations by Anisotropic Metamaterials, *Phys. Rev. Lett.* **99**, 063908 (2007).
- [59] M. Q. Mehmood, S. Mei, S. Hussain, K. Huang, S. Y. Siew, L. Zhang, T. Zhang, X. Ling, H. Liu, J. Teng, A. Danner, S. Zhang, and C.-W. Qiu, Visible-frequency metasurface for structuring and spatially multiplexing optical vortices, *Adv. Mater.* **28**, 2533 (2016).
- [60] C. Pfeiffer, C. Zhang, V. Ray, L. J. Guo, and A. Grbic, High Performance Bianisotropic Metasurfaces: Asymmetric Transmission of Light, *Phys. Rev. Lett.* **113**, 023902 (2014).
- [61] J. Kaschke, J. K. Gansel, and M. Wegener, On metamaterial circular polarizers based on metal N-helices, *Opt. Express* **20**, 26012 (2012).
- [62] H. L. Zhu, S. W. Cheng, K. L. Chung, and T. I. Yuk, Linear-to-circular polarization conversion using metasurface, *IEEE Trans. Antennas. Propag.* **61**, 4615 (2013).
- [63] Y. Li, J. Zhang, S. Qu, J. Wang, L. Zheng, Y. Pang, Z. Xu, and A. Zhang, Achieving wide-band linear-to-circular polarization conversion using ultra-thin bi-layered metasurfaces, *J. Appl. Phys.* **117**, 044501 (2015).
- [64] W.-L. Guo, G.-M. Wang, K. Chen, H.-P. Li, Y.-Q. Zhuang, H.-X. Xu, and Y. Feng, Broadband Polarization-Conversion Metasurface for a Cassegrain Antenna with High Polarization Purity, *Phys. Rev. Appl.* **12**, 014009 (2019).
- [65] Y. Yang, W. Wang, P. Moitra, I. I. Kravchenko, D. P. Briggs, and J. Valentine, Dielectric meta-reflectarray for broadband linear polarization conversion and optical vortex generation, *Nano Lett.* **14**, 1394 (2014).
- [66] Y. Zhao, B. Qi, T. Niu, Z. Mei, L. Qiao, and Y. Zhao, Ultra-wideband and wide-angle polarization rotator based on double W-shaped metasurface, *AIP Adv.* **9**, 085013 (2019).
- [67] R. T. Ako, W. S. L. Lee, M. Bhaskaran, S. Sriram, and W. Withayachumankul, Broadband and wide-angle reflective linear polarization converter for terahertz waves, *AIP Photonics* **4**, 096104 (2019).
- [68] H. Sun, C. Gu, X. Chen, Z. Li, L. Liu, and F. Martín, Ultra-wideband and broad-angle linear polarization conversion metasurface, *J. Appl. Phys.* **121**, 174902 (2017).